Dark-field optical tweezers for nanometrology of metallic nanoparticles

Kellie Pearce,[1] **Fan Wang,**[1] **and Peter J. Reece**[1,*]

[1]*School of Physics, The University of New South Wales, Sydney, NSW 2052, Australia*

[*]*p.reece@unsw.edu.au*

Abstract: Applications of metallic nanoparticles are based on their strongly size-dependent optical properties. We present a method for combining optical tweezers with dark field microscopy that allows measurement of localised surface plasmon resonance (LSPR) spectra on single isolated nanoparticles without compromising the strength of the optical trap. Using this spectroscopic information in combination with measurements of trap stiffness and hydrodynamic drag, allows us to determine the dimensions of the trapped nanoparticles. A relationship is found between the measured diameters of the particles and the peak wavelengths of their spectra. Using this method we may also resolve complex spectra of particle aggregation and interactions within the tweezers.

OCIS codes: (355.4855) Optical tweezers and optical micromanipulation; (250.5403) Plasmonics; (160.4236) Nanomaterials.

References and links

1. F. Hajizadeh and S. S.Reihani, "Optimized optical trapping of gold nanoparticles," Opt. Express **18**(2), 551–559 (2010). URL http://www.opticsexpress.org/abstract.cfm?URI=oe-18-2-551.
2. M. Guffey and N. Scherer, "All-optical positioning of single and multiple Au nanoparticles on surfaces using optical trapping," Proc. SPIE **7762**(1) (2010). URL http://dx.doi.org/10.1117/12.871881.
3. A. F. Koenderink, "Plasmon nanoparticle array waveguides for single photon and single plasmon sources," Nano Letters **9**(12), 4228–4233 (2009). PMID: 19835368, http://pubs.acs.org/doi/pdf/10.1021/nl902439n, URL http://pubs.acs.org/doi/abs/10.1021/nl902439n.
4. J. N. Anker, W. P. Hall, O. Lyandres, N. C. Shah, J. Zhao, and R. P. Van Duyne, "Biosensing with plasmonic nanosensors," Nat Mater **7**(6), 442–453 (2008). URL http://dx.doi.org/10.1038/nmat2162.
5. R. P. Van Duyne, A. J. Haes, and A. D. McFarland, "Nanoparticle optics: fabrication, surface-enhanced spectroscopy, and sensing," SPIE Proc. **5223**, 197–207 (2003). URL http://link.aip.org/link/?PSI/5223/197/1.
6. C. Sönnichsen, T. Franzl, T. Wilk, G. von Plessen, and J. Feldmann, "Plasmon resonances in large noble-metal clusters," New J Phys **4**(1), 93 (2002). URL http://stacks.iop.org/1367-2630/4/i=1/a=393.
7. T. Itoh, T. Uwada, T. Asahi, Y. Ozaki, and H. Masuhara, "Analysis of localized surface plasmon resonance by elastic light-scattering spectroscopy of individual Au nanoparticles for surface-enhanced Raman scattering," Can J Anal Sci Spectros **52**, 130–141 (2007).
8. H. Tamaru, H. Kuwata, H. T. Miyazaki, and K. Miyano, "Resonant light scattering from individual Ag nanoparticles and particle pairs," App Phys Lett **80**(10), 1826–1828 (2002). URL http://link.aip.org/link/?APL/80/1826/1.
9. J. Prikulis, F. Svedberg, M. Käll, J. Enger, K. Ramser, M. Goksör, and D. Hanstorp, "Optical spectroscopy of single trapped metal nanoparticles in solution," Nano Lett **4**(1), 115–118 (2004). http://pubs.acs.org/doi/pdf/10.1021/nl0349606, URL http://pubs.acs.org/doi/abs/10.1021/nl0349606.
10. F. Gittes and C. F. Schmidt, "Interference model for back-focal-plane displacement detection in optical tweezers," Opt. Lett. **23**(1), 7–9 (1998). URL http://ol.osa.org/abstract.cfm?URI=ol-23-1-7.

#155371 - $15.00 USD Received 3 Oct 2011; revised 10 Nov 2011; accepted 11 Nov 2011; published 30 Nov 2011

11. M. Dienerowitz, M. Mazilu, and K. Dholakia, "Optical manipulation of nanoparticles: a review," J Nanophot **2**, 021875 (pages 32) (2008). URL http://link.aip.org/link/?JNP/2/021875/1.
12. L. Tong, V. D. Miljkovic, and M. Kall, "Optical manipulation of plasmonic nanoparticles using laser tweezers," Proc. SPIE **7762**, 77,620O–8 (2010). URL http://link.aip.org/link/?PSI/7762/77620O/1.
13. Z. Jin-Hua, Q. Lian-Jie, Y. Kun, Z. Min-Cheng, and L. Yin-Mei, "Observing nanometre scale particles with light scattering for manipulation using optical tweezers," Chin Phys Lett **25**(1), 329 (2008). URL http://stacks.iop.org/0256-307X/25/i=1/a=088.
14. P. J. Reece, W. J. Toe, F. Wang, S. Paiman, Q. Gao, H. H. Tan, and C. Jagadish, "Characterization of semiconductor nanowires using optical tweezers," Nano Lett **11**(6), 2375–2381 (2011). URL http://pubs.acs.org/doi/abs/10.1021/nl200720m.
15. D. Selmeczi, P. H. Hagedorn, S. Mosler, N. B. Larsen, and H. Flyvbjerg, "Brownian motion after Einstein and Smoluchowski : some new applications and new experiments," Acta Physica Polonica B **38**(8), 2407–2431 (2007).
16. K. C. Neuman and S. M. Block, "Optical trapping," Rev Sci Instrum **75**(9), 2787–2809 (2004). URL http://link.aip.org/link/?RSI/75/2787/1.
17. V. Rudyak, A. Belkin, and E. Tomilina, "Force acting on a nanoparticle in a fluid," Tech Phys Lett **34**(1), 76–78 (2008-01-01). URL http://dx.doi.org/10.1134/S1063785008010239.
18. R. P. Carney, J. Y. Kim, H. Qian, R. Jin, H. Mehenni, F. Stellacci, and O. M. Bakr, "Determination of nanoparticle size distribution together with density or molecular weight by 2D analytical ultracentrifugation," Nat Commun **2** (2011). URL http://dx.doi.org/10.1038/ncomms1338.
19. K. A. Willets and R. P. Van Duyne, "Localized surface plasmon resonance spectroscopy and sensing," Annu Rev Phys Chem **58**(1), 267–297 (2007). URL http://www.annualreviews.org/doi/abs/10.1146/annurev.physchem.58.032806.104607.
20. A. Haes, C. Haynes, A. McFarland, G. Schatz, R. V. Duyne, and S. Zou, "Plasmonic materials for surface-enhanced sensing and spectroscopy," MRS Bulletin **30**, 368–375 (2005). URL http://dx.doi.org/doi:10.1557/mrs2005.100.
21. S. Link and M. A. El-Sayed, "Spectral properties and relaxation dynamics of surface plasmon electronic oscillations in gold and silver nanodots and nanorods," J Phys Chem B **103**(40), 8410–8426 (1999). URL http://pubs.acs.org/doi/abs/10.1021/jp9917648.
22. K. L. Kelly, E. Coronado, L. L. Zhao, and G. C. Schatz, "The optical properties of metal nanoparticles: the influence of size, shape, and dielectric environment," J Phys Chem B **107**(3), 668–677 (2003). URL http://pubs.acs.org/doi/abs/10.1021/jp026731y.
23. A. Tcherniak, J. W. Ha, S. Dominguez-Medina, L. S. Slaughter, and S. Link, "Probing a century old prediction one plasmonic particle at a time," Nano Lett **10**(4), 1398–1404 (2010). PMID: 20196552, URL http://pubs.acs.org/doi/abs/10.1021/nl100199h.
24. P. K. Jain, K. S. Lee, I. H. El-Sayed, and M. A. El-Sayed, "Calculated absorption and scattering properties of gold nanoparticles of different size, shape, and composition: applications in biological imaging and biomedicine," J Phys Chem B **110**(14), 7238–7248 (2006). PMID: 16599493, URL http://pubs.acs.org/doi/abs/10.1021/jp057170o.
25. C. Rayford, G. Schatz, and K. Shuford, "Optical properties of gold nanospheres," Nanoscape **2**, 27–33 (2005).
26. P. M. Hansen, V. K. Bhatia, N. Harrit, and L. Oddershede, "Expanding the optical trapping range of gold nanoparticles," Nano Lett **5**(10), 1937–1942 (2005). URL http://pubs.acs.org/doi/abs/10.1021/nl051289r.
27. A. Kyrsting, P. M. Bendix, D. G. Stamou, and L. B. Oddershede, "Heat profiling of three-dimensionally optically trapped gold nanoparticles using vesicle cargo release," Nano Lett **11**(2), 888–892 (2011). URL http://pubs.acs.org/doi/abs/10.1021/nl104280c.
28. S. Lal, S. E. Clare, and N. J. Halas, "Nanoshell-enabled photothermal cancer therapy: impending clinical impact," Acc Chem Res **41**(12), 1842–1851 (2008). http://pubs.acs.org/doi/pdf/10.1021/ar800150g, URL http://pubs.acs.org/doi/abs/10.1021/ar800150g.
29. L. Tong, V. D. Miljković, and M. Käll, "Alignment, rotation, and spinning of single plasmonic nanoparticles and nanowires using polarization dependent optical forces," Nano Lett **10**(1), 268–273 (2010). PMID: 20030391, URL http://pubs.acs.org/doi/abs/10.1021/nl9034434.
30. M. Pelton, M. Liu, H. Y. Kim, G. Smith, P. Guyot-Sionnest, and N. F. Scherer, "Optical trapping and alignment of single gold nanorods by using plasmon resonances," Opt. Lett. **31**(13), 2075–2077 (2006). URL http://ol.osa.org/abstract.cfm?URI=ol-31-13-2075.
31. C. Selhuber-Unkel, I. Zins, O. Schubert, C. Sönnichsen, and L. B. Oddershede, "Quantitative optical trapping of single gold nanorods," Nano Lett **8**(9), 2998–3003 (2008). PMID: 18720978, URL http://pubs.acs.org/doi/abs/10.1021/nl802053h.

#155371 - $15.00 USD Received 3 Oct 2011; revised 10 Nov 2011; accepted 11 Nov 2011; published 30 Nov 2011

1. Introduction

Metal nanoparticles exhibit unique size-dependent properties which govern their use in a wide variety of applications. Such applications include surface-enhanced Raman spectroscopy (SERS), cancer detection and treatment, chemical and biological sensing, and optical antennas. [1–3] In the case of nano-sized biosensors, the use of single-particle sensors offers the highest spatial resolution and reduced absolute detection limits [4, 5]. Many more potential applications exist which – particularly in the case of single-particle applications – require correlations to be made between individual geometries and optical properties.

The phenomenon of localised surface plasmon resonance (LSPR) is responsible for the local electric field enhancement and strong scattering exhibited by metallic nanoparticles. The peak wavelength, width and intensity of the scattering spectra are highly dependent on several factors including the size and shape of the particle and its local dielectric environment, making spectroscopy a sensitive probe of these features.

To date, the majority of LSPR studies have been performed on colloidal ensembles of particles which – due to the distribution of sizes and shapes within the sample – produce inhomogeneously broadened spectra, obscuring individual optical properties. Strong correlations can only be made between spectral features and individual geometries if particles are able to be isolated and single-particle spectra obtained. Several authors have achieved this isolation using spin coating to fix particles to glass substrates [6–8], followed by covering the substrate with a medium such as water or immersion oil. However, the proximity of the particle to the substrate changes the local dielectric environment and therefore the resulting spectra, an effect which can be difficult to account for.

It has been noted in previous single-particle LSPR studies that there is a variation in peak wavelengths amongst individual particles, which was attributed to the distribution of particle shapes and sizes around the nominal diameter [2, 7, 9]. This size distribution can be confirmed by electron microscopy measurements, but these limit the correlation that can be made between the size of an individual particle and its optical properties. It would be advantageous to have a technique which is able to determine the size of a single nanoparticle in solution and observe its scattering spectrum simultaneously.

Optical tweezers have long been used to isolate single micron and nano-sized objects and study their physical properties. The strength of the optical trap for each object is quantified by a value known as the trap stiffness, which can be determined through analysis of the object's motion within the trap. We present a method of determining the size of a trapped nanoparticle through the comparison of two methods for obtaining the trap stiffness. Additionally, we demonstrate a method of incorporating a dark field illumination scheme into an optical tweezers setup which does not compromise the strength of the optical trap. This allows us to perform LSPR spectroscopy on a single trapped particle in conjunction with size measurements.

2. Experimental

A schematic diagram of the experimental set-up used for this study is presented in Fig. 1(a). The optical tweezers comprise of a linearly polarised 5 W, CW Nd:YAG laser (Laser Quantum, 1064 Ventus, λ = 1064nm, TEM_{00}), which is focused using an oil-immersion microscope objective (Olympus, E-plan 100×, NA = 1.25), via relay optics, in order to create a diffraction limited spot in the front focal plane. A two-axis acousto-optic (AO) deflector (NEOS Technologies) provides automated control of the position of the laser within the objective's field-of-view with a fast response time. A half-wave plate and polarizing beam splitter is used to control the power of the beam, and a second wave plate is used to control the polarisation in the focal plane. The absolute power at the focus is measured using a calibrated photodetector (Coherent

#155371 - $15.00 USD Received 3 Oct 2011; revised 10 Nov 2011; accepted 11 Nov 2011; published 30 Nov 2011

Fieldmaster) taking into account the transmission losses of the optical system and microscope objective. A position sensitive detector (PSD, Silicon Pacific Sensors) was used to observe the position fluctuations of objects within the trap by relating the displacement from the centre to the interference pattern formed at the back focal plane [10]. A field programmable gate array (FPGA)-based data acquisition card is used to synchronize the switching of the AO deflector and the detector.

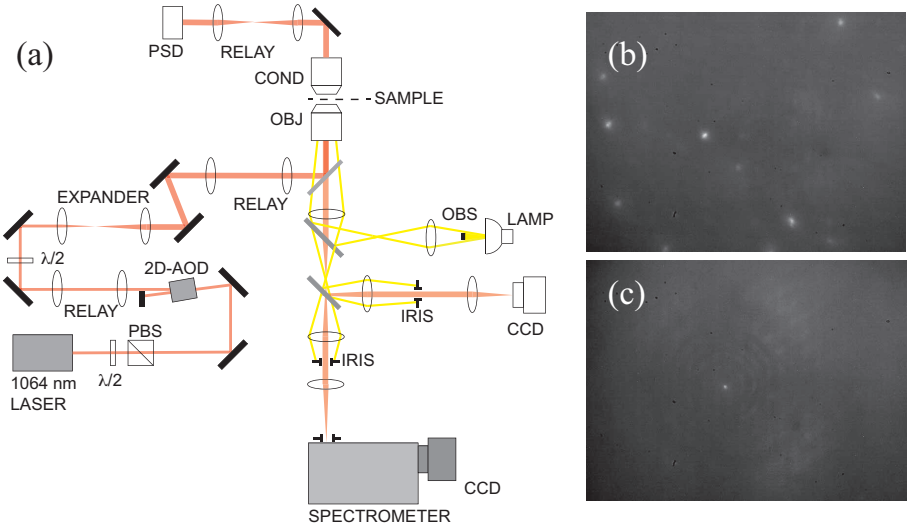

Fig. 1. (a) Optical tweezers setup that incorporates dark-field microscopy / spectroscopy. The illuminating light is formed into a ring by placing a custom-made block after the light source. The image of this ring is projected onto the sample; its reflection is blocked from entering the CCD camera by using an aperture, allowing only the scattered light to pass. (b) Dark field images of freely moving 200nm particles, (c) a trapped 100nm particle.

Incorporating a typical dark field illumination scheme into an optical tweezers setup poses some difficulties [11]. To achieve a strong gradient force a high NA objective must be used, yet to perform conventional diascopic dark field microscopy the NA of the objective must be lower than that of the condenser. Presently, dark field studies on optically trapped objects have been performed by either tolerating a lower NA objective [9,12], or using a laser beam perpendicular to the sample as the illumination source [13]. However, the former setup suffers from a reduced trapping strength, the later from an inability to perform spectroscopic measurements.

In our setup, we achieve dark field microscopy by using backscattered light to image the sample. A custom-made circular block was placed in front of the light source to form a ring of light which was imaged onto the back focal plane of the objective. The reflected ring was excluded from being collected by the CCD camera or spectrometer (Acton SP2300 & PIXIS 256, Princeton Instruments) by placing a circular aperture before each of these elements. Fig. 1(b) shows a dark-field micrograph image of 200nm metallic nanoparticles freely moving under Brownian motion and Fig. 1(c) displays trapped 100nm metallic nanoparticle under the same illumination conditions.

Gold nanoparticles of nominal sizes 60, 80, 100, and 150 were available for study, synthesised by BBInternational. Samples were diluted with milli-Q water from stock solution to ensure that only one particle enters the tweezers during the course of the measurements. A 5 μL volume of the nanoparticle suspension was pipetted into a sealed microfluidic chamber with a height of approximately 100 μm. Trapping measurements were performed on individual

#155371 - $15.00 USD Received 3 Oct 2011; revised 10 Nov 2011; accepted 11 Nov 2011; published 30 Nov 2011

nanoparticles at a height of approximately 10 μm from the cover slip. Trapping powers ranged from 40mW to 150mW.

The trap stiffness κ was derived from a time series of PSD readings via two methods, which are described in greater detail in the following section. One of these methods required the trap to be calibrated, that is, a given PSD reading to be associated with a known distance of the particle away from the centre of the trap. For small displacements of the object from the centre of the trap, the detector response is linear [10]. Calibration curves were obtained by using the AO deflector to move the particle a given distance away from its original position then quickly (15-20 μs) switching the laser back to the centre and recording the detector response. The time in which the PSD response was recorded needed to be sufficiently short so that the particle did not diffuse a significant distance away from its given position. This technique had previously been shown to obtain good results for 1μm polystyrene spheres and semiconductor nanowires with our setup [14]. After trap calibration, time series data of the Brownian motion of the trapped particles was recorded for 2.5 seconds at a sampling rate of 40 kHz using the PSD connected to a data acquisition card. Low pass filtering was used to remove the non-thermal component of the particle motion.

3. Theory

Determination of the optical forces on trapped objects uses the fact that the system can be considered as a highly overdamped simple harmonic oscillator [11]. The trapping beam creates a parabolic potential well, so that the restoring force can be described using Hooke's law: $\mathbf{F} = -\kappa\mathbf{x}$ for which the trap stiffness κ can be calculated.

The particle undergoes Brownian motion, described by a Langevin equation within a trapping medium where viscous forces dominate. The thermal force *F(t)* is given in the Einstein-Ornstein-Uhlenbeck theory by $F(t) = (2k_bT\gamma_o)^{1/2}\eta(t)$ where $\eta(t)$ is a white noise term such that $\langle\eta(t)\rangle = 0$ and the autocorrelation function is a delta-function [15].

Using these, the Langevin equation becomes

$$\gamma_o\frac{\partial x}{\partial t} + \kappa x = (2k_bT\gamma_o)^{1/2}\eta(t). \tag{1}$$

The first method used to obtain the trap stiffness κ, called the *power spectrum method,* takes the Fourier transform of the above equation giving,

$$\hat{x} = \frac{(2k_bT\gamma_o)^{1/2}\hat{\eta}}{2\pi(f_c - if)} \tag{2}$$

where $\hat{\eta}$ is the Fourier transform of the white noise term. This gives a Lorentzian power spectrum [16],

$$S(f) \equiv \left\langle \frac{|\hat{x}^2|}{T} \right\rangle = \frac{k_bT}{\pi^2\gamma(f_c^2 + f^2)}. \tag{3}$$

In the above equations the *corner frequency* is

$$f_c \equiv \frac{\kappa}{2\pi\gamma_o}, \tag{4}$$

which can be used to obtain the trap stiffness κ if the viscous drag coefficient γ is known. For a sphere of diameter d moving through a fluid with viscosity η the drag coefficient is given by Stoke's law

$$\gamma_o = 3\pi\eta d. \tag{5}$$

#155371 - $15.00 USD Received 3 Oct 2011; revised 10 Nov 2011; accepted 11 Nov 2011; published 30 Nov 2011

The applicability of Stoke's law begins to break down for nanoparticles of a sufficiently small size, where intermolecular forces dominate the particles' behaviour [17, 18]. However, this regime (smaller than a few nanometers) is well below the sizes of particles investigated in this project and so Stoke's law is always assumed to hold for spherical objects. We also assume the Flaxan correction is small as the diameter of the particle - of the order of 100 nm - is much smaller than the distance from the cover glass to the trapping height.

The second method of obtaining κ, called the *Gaussian method*, uses the fact that the probability of displacement of a particle in a potential well with potential energy *U(x)* is given by the Boltzmann distribution, which becomes a Gaussian for a parabolic potential

$$P(x) \propto \exp\left(\frac{-U(x)}{k_b T}\right) = \exp\left(\frac{-\kappa x^2}{2k_b T}\right). \tag{6}$$

Unlike the power spectrum method there is no explicit dependence on the drag, so the shape of the particle, its proximity to a surface, and the viscosity of the trapping medium do not need to be known. However, this method requires the calibration described in the previous section.

In a calibrated trap the power spectrum and Gaussian method can used to obtain two values for the trap stiffness simultaneously, which are equal for an object of known size. If the diameter is assumed to be unknown, the trap stiffness given by the Gaussian method and the corner frequency can be used to estimate the size of the trapped particle. The calculated diameter d is

$$d = \frac{\kappa_G}{6\pi^2 f_c \eta}. \tag{7}$$

For metal nanoparticles, the wavelength-dependent extinction (absorption plus scattering) spectrum is given by [19, 20]

$$E(\lambda) = \frac{24\pi^2 N a^3 \varepsilon_{out}^{3/2}}{\lambda \, ln(10)} \left[\frac{\varepsilon_i(\lambda)}{\varepsilon_r(\lambda) + \chi \varepsilon_{out}(\lambda)^2}\right], \tag{8}$$

where ε_r and ε_i are the real and imaginary components of the dielectric function of the metal respectively, ε_{out} is the dielectric constant external environment, a is the particle radius, and N is the number of polarizable elements that the particle can be represented by. The factor χ is equal to 2 in the case of a sphere, but increases for particle geometries with high aspect ratios [21]. This factor is only able to be analytically calculated for spheres and spheroids (where two axes are equal); other attempts to determine the extinction spectrum rely on approximations, which typically are reasonable matches to experimental results [21, 22].

4. Results and discussion

The method described above for determining the size of a trapped spherical object was first tested on 1μm polystyrene spheres. It was shown that the correct diameters were obtained, and furthermore that the results remained the same over a wide range of trapping powers due to the power independence of the Gaussian method for these objects.

The same method was used to determine the relationship between the slope of the calibration curve and the power of the trapping laser for gold nanospheres of 100nm nominal diameter. Results are shown in Fig. 2. In Fig. 2(a) the calibration curve is shown for nanoparticle displacements of $\pm$120nm from the centre of the trap, for different trapping powers. In this region the detector provides response that is linearly proportional to the particle displacement. As the detector response is normalized to the sum of the signal measured by the PSD we expect that under normal operating conditions the slope of the response should be independent of the trapping power. However, we see from a plot of the calibration gradient of the calibration as a

#155371 - $15.00 USD Received 3 Oct 2011; revised 10 Nov 2011; accepted 11 Nov 2011; published 30 Nov 2011

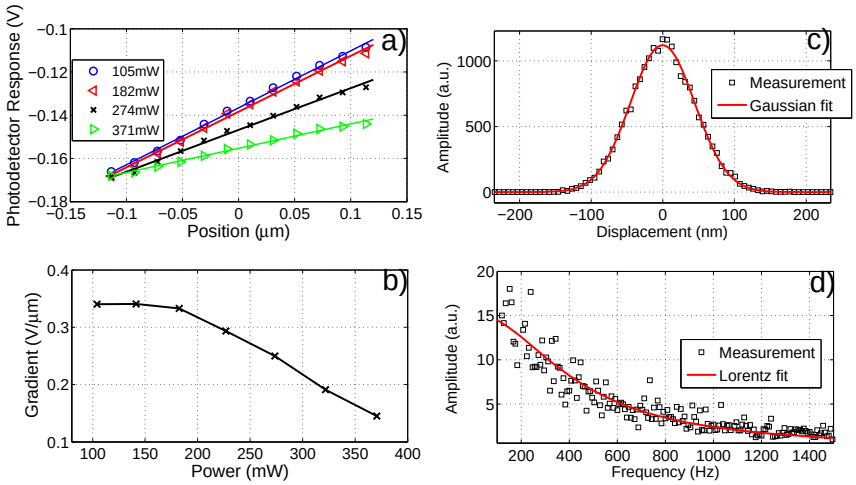

Fig. 2. (a) Position sensitive detector calibration curves for 100nm particles at various trapping powers. (b) The gradient of each curve as a function of the trapping power. Below powers of around 75mW the gradient is power independent. Above this, increasing power decreases the gradient of the curve. (c) Histogram showing the Brownian fluctuations of a optically trapped nominally 100nm nanoparticle using a trapping power of 65 mW at the focus. The histogram was fitted with a Gaussian model and the trapping value was calculated as 2.15 pN / μ m. (d) The power spectrum data for the same time series was fitted to a Lorentzian curve giving a corner frequency of 405 Hz. Using Eq. (7) we estimate that the size of the particle to be 94 nm.

function of trapping power, presented in Fig. 2(b), that below a power of 75mW the gradient of the calibration curve was independent of the slope, so the Gaussian and power spectrum methods would give consistent results, allowing valid size measurements to be made.

However, for powers above 75mW, the gradient of the calibration curve decreased with increasing power. This would lead to an underestimate of the trap stiffness via the Gaussian method, and consequently a measured diameter smaller than the true diameter according to Equation (7). This power dependence is thought to be due to the movement of the particles during the measurement time, when the laser has been moved back to the central position. Since this movement is a result of Brownian motion, in zero external potential it will be random, so the effect of averaging many measurements will produce no mean displacement. However, if the particle is located near a strong attractive potential – which is created by increasing the laser power – the particle will tend to drift back towards the central position. The detector response is therefore recorded for an object that is closer to the centre than the position it was placed at, causing the measured calibration curve to be shallower than the true curve.

It was necessary to avoid this effect when performing size measurements, so the trapping power used was as small as possible. The effect could also be reduced by keeping the measurement time low.

Typical trapping measurements for a 100 nm gold nanoparticle are shown in Fig. 2(c)-(d). These measurements were done using a power of 65 mW at the focal plane. From the time series trace of the particle motion a histogram is built of the displacement of the particle with respect to the centre of the trap. Using a Gaussian fit to the data, the trapping stiffness was determined to be 0.033 $pN/\mu m/mW$. The corner frequency determined from a power spectrum analysis of the same sets of PSD readings is used to calculate the hydrodynamic diameter.

#155371 - $15.00 USD Received 3 Oct 2011; revised 10 Nov 2011; accepted 11 Nov 2011; published 30 Nov 2011

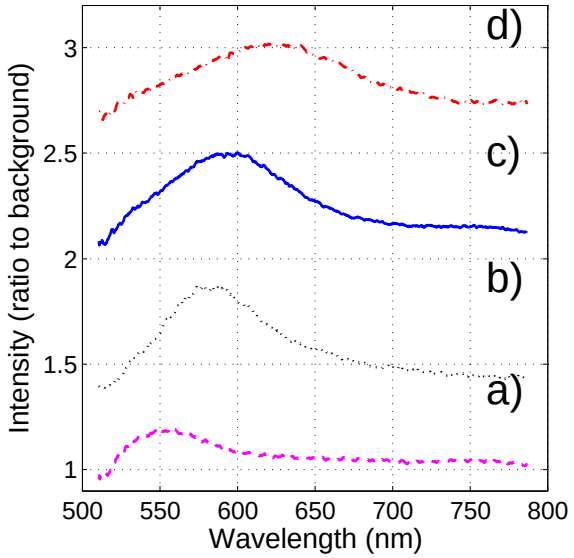

Fig. 3. Spectra obtained from trapped gold particles found in samples with nominal sizes 60, 80, 100 and 150nm (a-d). In the case of (d) the peak is at a shorter wavelength than expected, however, this can be explained by the observed distribution of particle sizes within each sample. With increasing particle size a redshift and broadening of the spectra can be seen.

In this instance the diameter of the particle was determined to be 94 nm. The inclusion of dark field illumination into the setup allowed scattering spectra to be obtained simultaneously, providing direct correlations between the size and the spectrum of the trapped particle. Typical LSPR spectra are presented in Fig. 3, demonstrating the redshift of the peak wavelength with increasing particle size.

The relationship established between measured diameters of particles and their peak LSPR scattering wavelengths is shown in Fig. 4. The average error in the measured diameters for these particles was 6.4%. This was estimated by repeating a number of time series measurements on the same nanoparticle and using the standard deviation to determine the error. To compare these results with previous work, values of the peak wavelengths for a few different particle sizes were taken from several theoretical calculations [23–25], and one published experimental result [12]. Only a small number of theoretical studies have attempted to separate the single-particle scattering spectra from the extinction spectra, so comparisons are somewhat limited. However, it can be seen that for particles larger than 60nm our results agree with those previously calculated within errors. For particles smaller than this size the results diverge, with our measurements giving a higher peak wavelength than expected for those sizes. It is noted that the comparison of hydrodynamic diameter and LSPR peak wavelength for the 150nm nanoparticles is not included Fig. 4. The reason for this is that the dwell time of the 150nm particles in the trap, before they escape, is not long enough to collect all of the necessary data (i.e. dark field spectrum, calibration and time series acquisition) to make the comparison. With further improvements to the optical tweezers set-up the trapping range may be extended to the large particles sizes (up to 250nm).

We propose that this discrepancy is due to significant heating of the smaller nanoparticles, as higher trapping powers need to be used as the size of the particles decreases [26]. Further to

#155371 - $15.00 USD Received 3 Oct 2011; revised 10 Nov 2011; accepted 11 Nov 2011; published 30 Nov 2011

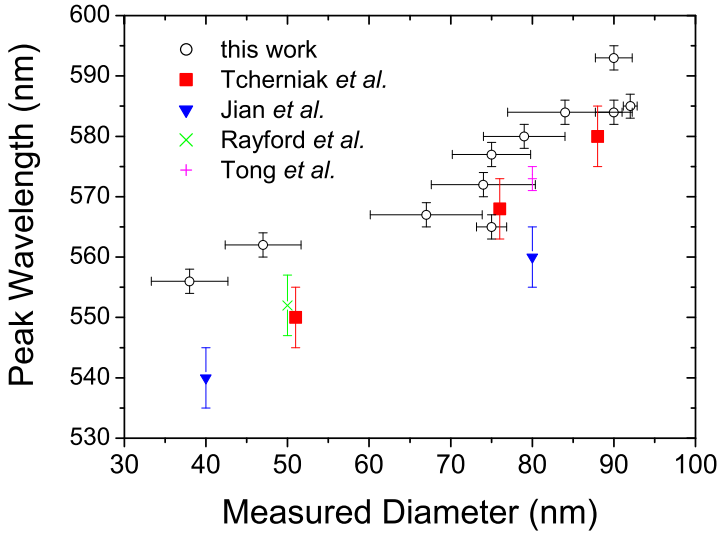

Fig. 4. Peak wavelengths of the LSPR spectra of gold nanoparticles as a function of their measured diameters. Particles from samples with nominal diameters 60, 80 and 100nm. The sizes are measured based on the optical trapping power spectrum and equipartition measurements. Also shown are data of size correlated LSPR spectra from previous studies.

this, it has been found that the heating of trapped small particles is greater than that for larger particles [27]. The amount of heating is estimated by first calculating the size, d, based on the LSPR resonance peak (using the published data as a reference), then using this to determine the trap stiffness κ using the power spectrum method, and finally using the Gaussian method (Eqn.(6)) to infer the temperature increase required to give the same distribution. If we assume the theoretical values for the LSPR peaks are correct, we estimate a heating of 142°C and 109°C for the particles measured to be 38 and 47nm respectively. T For a trapping power of 200mW, this equates to 710°C/W and 545°C/W – values of the same order as those found by other authors [27]. The determination of heating due to laser interactions of nanoparticles, particularly with the emergence of applications of cancer therapy in nanomedicine [28], is becoming increasingly important. The method presented here for trapped objects with well characterised LSPR spectral properties offers the unique possibility of studying heating of particles using a range of stimuli and under different environmental conditions.

By combining size and spectroscopic measurements, we were also able to identify situations in which multiple particles or particle aggregates were trapped. If, after calibration, a second object fell into the trap the trap-stiffness measured via the Gaussian method was halved, resulting in a measured diameter twice that of a single particle. The scattering spectrum of the doubly-trapped particles was redshifted from that of a single gold sphere – the result of plasmon coupling which occurs at close distances (a few times the particle diameter). Figure 5(a) demonstrates the redshift (580→595nm) and increased scattering intensity observed when a second particle enters the trap. In this case the particles had nominal diameters of 80nm. Evidence for clumping could be seen via the dark field images and via the spectra. White light scattering from aggregates of gold particles often spread out over many pixels and produced unusual spectra; an example of which is shown in Fig. 5(b) inset. The complex spectrum on the

#155371 - $15.00 USD Received 3 Oct 2011; revised 10 Nov 2011; accepted 11 Nov 2011; published 30 Nov 2011

left was taken from a larger cluster, similar in appearance to that shown in Fig. 5(b), which was stuck onto the surface of the glass slide. The spectrum on the right was from a large trapped particle. Double peaks correspond to dipole and quadrupole resonances, which appear in particles of sufficiently large sizes.

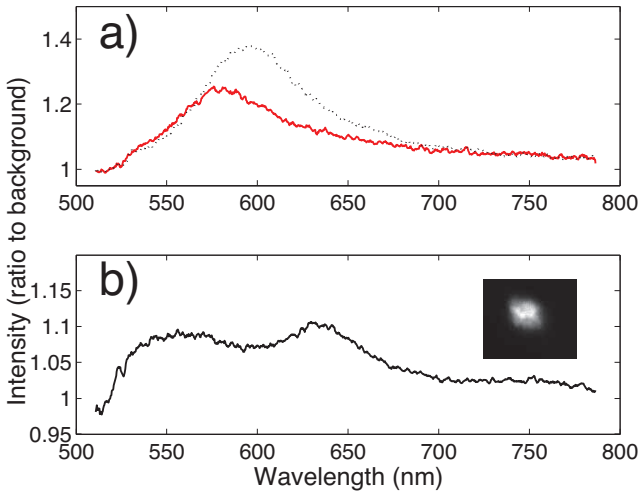

Fig. 5. (a) The LSPR spectrum of a trapped gold particle of nominal diameter 80nm (red) and (black) the altered spectrum when a second particle enters the trap. Both a redshift of the peak and an increase in scattered intensity can be seen. (b) a complex LSPR spectrum of an optically trapped particle aggregate showing higher order resonances. An example of a cluster of particles as observed under dark field imaging is represented in the inset.

In the case of particle aggregates becoming trapped, the measured diameter was also larger than expected for the nominal size of the sample. However, aggregates were easy to distinguish from multiply-trapped single particles, even if not obvious by their appearance, since their larger sizes and non-spherical shapes gave rise to complex spectra and larger size measurement errors. Scattering spectra of these objects often displayed double peaks corresponding to the excitation of both dipole and quadrupole plasmon resonances, or had long peak wavelengths which suggested an elongated shape [22].

This technique could be applied to non-spherical nanoparticles such as nanorods, by exploiting the tendency of the longer axis to align to the polarization of the trapping beam [29–31]. Trap stiffness measurements could be made along both the x and y directions to obtain the dimensions of the particle along these axes. These would then be correlated with each of the dual plasmon bands observed in elongated objects which correspond to resonances along the width and length of the particle.

5. Conclusion

We have shown that the sizes of optically trapped nanoparticles can be determined by measuring their trapping properties via two different methods. This provides a relatively simple way of determining the diameters of individual particles in solution. Furthermore, we established a dark field illumination scheme which is able to be applied to trapped objects without reducing the trapping strength. The combination of these two techniques allowed the results single-particle spectroscopy to be correlated with the sizes of individual particles, an ability which may be

#155371 - $15.00 USD Received 3 Oct 2011; revised 10 Nov 2011; accepted 11 Nov 2011; published 30 Nov 2011

necessary for potential applications.

Our setup also allowed us to easily identify particle aggregates and observe the redshift in the LSPR spectra when multiple objects become trapped. There is the possibility to extend this technique to non-spherical objects in the future.

Acknowledgement

We would like to acknowledge V. Coleman of the Australian National Measurement Institute for providing the materials and for useful discussions.

#155371 - $15.00 USD Received 3 Oct 2011; revised 10 Nov 2011; accepted 11 Nov 2011; published 30 Nov 2011